

Current Biology

Brain wiring determinants uncovered by integrating connectomes and transcriptomes

Highlights

- Transcriptome-connectome map of the *Drosophila* motion detection circuit
- Expression of Side/Beat receptor-ligand pairs correlates with synaptic specificity
- Side-II/Beat-VI pair restricts synaptic partners to the same layer of neuropil

Authors

Juyoun Yoo, Mark Dombrovski, Parmis Mirshahidi, Aljoscha Nern, Samuel A. LoCascio, S. Lawrence Zipursky, Yerbol Z. Kurmangaliyev

Correspondence

lzipursky@mednet.ucla.edu (S.L.Z.),
yerbol@brandeis.edu (Y.Z.K.)

In brief

Yoo et al. combine synaptic connectome, single-cell transcriptome, and protein interactome maps to identify brain wiring determinants in the *Drosophila* visual system. Matching expression of Side-II/Beat-VI receptor-ligand pair in pre- and postsynaptic partners regulates wiring specificity in the directionally selective motion detection circuit.



Report

Brain wiring determinants uncovered by integrating connectomes and transcriptomes

Juyoun Yoo,^{1,2} Mark Dombrovski,¹ Parmis Mirshahidi,¹ Aljoscha Nern,³ Samuel A. LoCasio,¹ S. Lawrence Zipursky,^{1,*} and Yerbol Z. Kurmangaliyev^{1,4,5,*}

¹Department of Biological Chemistry, Howard Hughes Medical Institute, David Geffen School of Medicine, University of California, Los Angeles, Los Angeles, CA 90095, USA

²Neuroscience Interdepartmental Program, University of California, Los Angeles, Los Angeles, CA 90095, USA

³Janelia Research Campus, Howard Hughes Medical Institute, Ashburn, VA 20147, USA

⁴Present address: Department of Biology, Brandeis University, Waltham, MA 02453, USA

⁵Lead contact

*Correspondence: lzzipursky@mednet.ucla.edu (S.L.Z.), yerbol@brandeis.edu (Y.Z.K.)

<https://doi.org/10.1016/j.cub.2023.08.020>

SUMMARY

Advances in brain connectomics have demonstrated the extraordinary complexity of neural circuits.^{1–5} Developing neurons encounter the axons and dendrites of many different neuron types and form synapses with only a subset of them. During circuit assembly, neurons express cell-type-specific repertoires comprising many cell adhesion molecules (CAMs) that can mediate interactions between developing neurites.^{6–8} Many CAM families have been shown to contribute to brain wiring in different ways.^{9,10} It has been challenging, however, to identify receptor-ligand pairs directly matching neurons with their synaptic targets. Here, we integrated the synapse-level connectome of the neural circuit^{11,12} with the developmental expression patterns⁷ and binding specificities of CAMs^{6,13} on pre- and postsynaptic neurons in the *Drosophila* visual system. To overcome the complexity of neural circuits, we focus on pairs of genetically related neurons that make differential wiring choices. In the motion detection circuit,¹⁴ closely related subtypes of T4/T5 neurons choose between alternative synaptic targets in adjacent layers of neuropil.¹² This choice correlates with the matching expression in synaptic partners of different receptor-ligand pairs of the Beat and Side families of CAMs. Genetic analysis demonstrated that presynaptic Side-II and postsynaptic Beat-VI restrict synaptic partners to the same layer. Removal of this receptor-ligand pair disrupts layers and leads to inappropriate targeting of presynaptic sites and postsynaptic dendrites. We propose that different Side/Beat receptor-ligand pairs collaborate with other recognition molecules to determine wiring specificities in the fly brain. Combining transcriptomes, connectomes, and protein interactome maps allow unbiased identification of determinants of brain wiring.

RESULTS AND DISCUSSION

Coupled transcriptome-connectome map of the *Drosophila* directionally selective motion detection circuit

Dense electron microscopy (EM) reconstructions identified most of the synaptic connections in the circuit that detects motion in different directions^{11,12} (Figures 1A and 1B). A set of eight closely related subtypes of T4/T5 neurons lie at its center. Each subtype is defined by a combination of one of two patterns of dendritic inputs and one of four patterns of axonal outputs (Figures 1A and 1F). T4 and T5 neurons arborize their dendrites in the medulla and lobula, respectively. Each of these groups is further subdivided into four subtypes (a/b/c/d) based on their axon terminals in four synaptic layers of the lobula plate (Lop1/2/3/4). Each pair of T4 and T5 neurons which project axons to the same layer respond optimally to motion in one cardinal direction; T4 neurons respond to the movement of bright edges (ON pathway) and T5 neurons respond to dark edges (OFF pathway).¹⁵ T4 and T5 axons

terminating in the same layer converge onto the same postsynaptic partners.¹² Furthermore, some of the postsynaptic neurons in different layers are also closely related cell types (see below). In this way, information from the ON (T4) and OFF (T5) pathways corresponding to each cardinal direction converge onto four parallel synaptic pathways (Figure 1B). We hypothesize that T4 and T5 subtypes, which form synapses with the same set of postsynaptic neurons in each layer of the lobula plate, do so through the same molecular mechanisms.¹⁶

To identify these molecules, we integrated the synaptic connectome and the transcriptome of developing neurons in the *Drosophila* visual system (Figures 1A–1C). We previously generated a comprehensive transcriptional atlas of the developing visual system using single-cell RNA sequencing.⁷ This atlas covers more than 160 neuronal populations at seven developmental time points; ~100 of them were matched to cell types in the connectome (Davis et al.¹⁷; A.N., Y.Z.K., and S.L.Z., unpublished data). This includes transcriptional profiles of all T4/T5 subtypes and 17 of their synaptic partners (Figure 1C). We focus on five types of



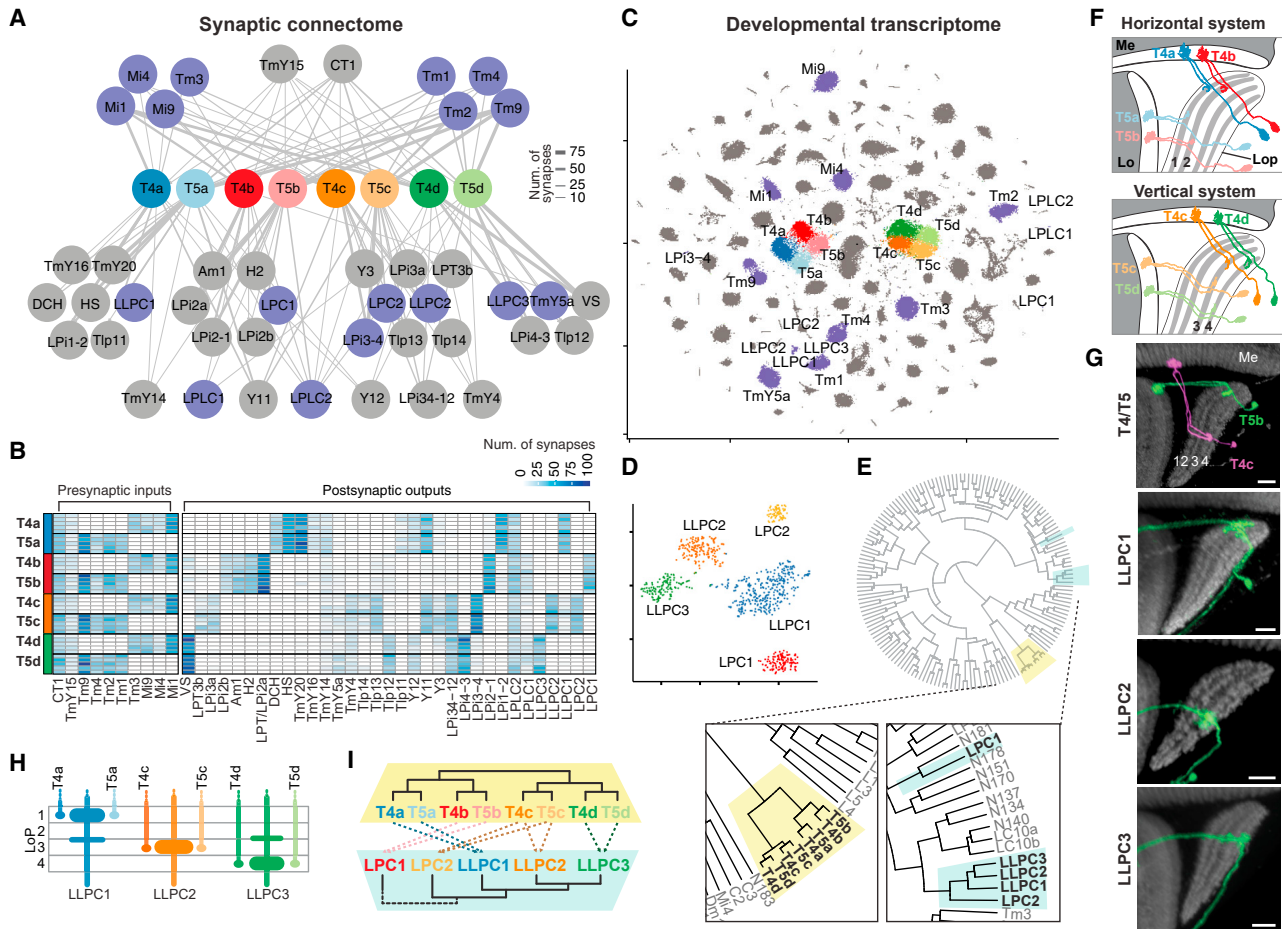


Figure 1. Coupled transcriptome-connectome map of the *Drosophila* circuit for directionally selective motion detection

(A and B) The connectome of T4/T5 subtypes from Shinomiya et al.¹¹ and Shinomiya et al.¹²
 (A) Cell-type-level connectome graph. Presynaptic inputs (top) and postsynaptic outputs (bottom) of T4/T5s are grouped and averaged by cell types. Purple, cell types with known transcriptomes.
 (B) Connectomes of individual T4/T5s, as an adjacency matrix. Five instances for each T4/T5 subtype (rows). Synaptic partners are grouped by cell type (columns). Each pair of T4 and T5 subtypes converge onto the same set of postsynaptic targets.
 (C) tSNE (t-distributed stochastic neighbor embedding) of the *Drosophila* visual system atlas.⁷ T4/T5s and their synaptic partners are labeled as in (A).
 (D) tSNE of the LPC/LLPC clusters.
 (E) Hierarchical clustering of transcriptomes in the visual system atlas; T4/T5 and LPC/LLPC neurons are shown in the zoom-in.
 (F) Morphology of eight T4/T5 subtypes. Me, medulla; Lo, lobula; LoP, lobula plate.
 (G) Sparsely labeled T4/T5s and LLPC neurons. Neuropil marker (gray), Brp. Scale bars, 10 μ m.
 (H) Synaptic connections between T4/T5 axons and LLPC dendrites are restricted to the layers of the lobula plate in which T4/T5 axons terminate. See also Figures 4D and S1.
 (I) Closely related pairs of T4 and T5 subtypes converge onto the same postsynaptic targets. See also Figure S1 and Table S1.

morphologically similar postsynaptic partners^{12,18}: two lobula plate columnar (LPC) and three lobula-lobula plate columnar (LLPC) neurons (Figures 1D and S1). Each of these neuron types receives its major input from one pair of T4 and T5 subtypes (in one layer of the lobula plate) (Figures 1B and 1G). In our initial version of the transcriptional atlas, these five cell types were not resolved. A more detailed analysis revealed distinct transcriptional clusters for each of them, which were validated by *in vivo* expression patterns of marker genes (Figure S1) and mRNA profiling of purified cell types (A.N., Y.Z.K., and S.L.Z., unpublished data). Hierarchical clustering of transcriptomes of all neuronal populations

in the visual system confirmed that the eight T4/T5 subtypes were closely related. Similarly, four LPC/LLPC types (except LPC1) were also closely related to each other (Figure 1E). Taken together, T4/T5 subtypes and LPC/LLPC types assemble into parallel synaptic pathways comprising homologous pairs of pre- and postsynaptic partners (Figures 1H and 1I).

Matching expression of Beat and Side proteins correlates with synaptic specificity

To understand how neurons choose their synaptic partners, we focused on connections between the most closely related T4/T5

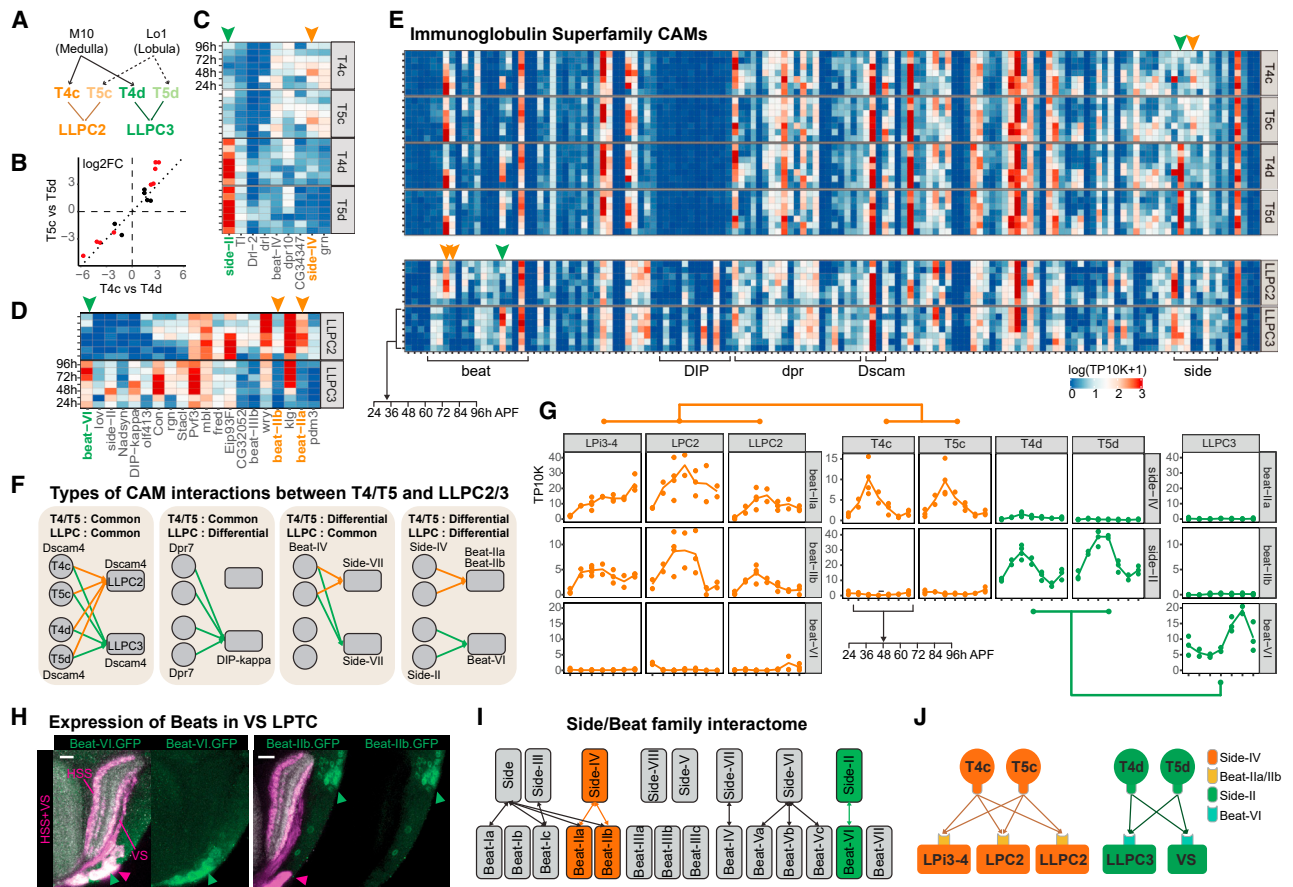


Figure 2. Matching expression of Beat and Side proteins correlates with synaptic specificity

(A) Connectome of T4/T5-LLPC2/3 circuit.

(B–D) Differentially expressed genes (DEGs) between T4/T5 and LLPC subtypes. See STAR Methods for details and thresholds.

(B) Log-fold change for DEGs between T4c and T4d (x axis), and T5c and T5d (y axis).

(C) Heatmap of expression patterns of DEGs significant in both comparisons in (B) (red).

(D) DEGs between LLPC2 and LLPC3.

(E) All annotated IgSF CAMs. Average expression levels are shown for seven time points after pupal formation (APF).

(F) Examples of matching CAM interactions between T4/T5 and LLPC. Only two pairs of interactors correlate with connectome: Side-IV::Beat-Ia/b and Side-II::Beat-VI (orange and green arrows in C–E).

(G) Line plots with average expression levels of these Beat/Side proteins in the T4/T5-LLPC2/3 circuit, and other major targets with known transcriptomes. Dots are replicates.

(H) *In vivo* expression of beat-Ib and beat-VI in VS neurons (adult), the main target of T4d/T5d (Figure 1D). Neuropil marker (gray), Brp. Scale bars, 10 μ m.

(I) Interactome of Beat/Side families from Li et al.⁶

(J) Matching receptor-ligand pairs between T4/T5s and their targets in Lop3 (orange) and Lop4 (green).

See also Figure S2 and Table S1.

pairs and their closely related postsynaptic targets, LLPC2 and LLPC3; T4c and T5c form synapses with LLPC2, and T4d and T5d form synapses with LLPC3 (Figure 2A). The transcriptional programs of these pairs of T4/T5 converge onto specific gene expression modules that correlate with the specificity of their axonal outputs.¹⁶ Most of the differentially expressed genes (DEGs) between T4c and T4d and between T5c and T5d were the same (Figure 2B). Of the nine shared DEGs, seven were cell surface proteins (Figure 2C). Nine cell adhesion molecules (CAMs) were differentially expressed between LLPC2 and LLPC3 neurons (Figure 2D). We hypothesize that CAMs that bind to each other and are specific to each pair of synaptic partners regulate their matching (e.g., T4d/T5d to LLPC3).

Although each T4/T5 subtype and LLPC types express many CAMs (Figure 2E), only two pairs of interacting CAMs correlated with synaptic specificities of these two sets of synaptic partners (Figure 2F). Both pairs belong to the Side and Beat families of immunoglobulin superfamily (IgSF) proteins, which form a heterophilic protein interaction network^{6,13} (Figure 2I). Founding members of these families (Side and Beat-Ia) were identified in genetic screens as regulators of motor axon guidance in the *Drosophila* embryo.^{19–21} Functions for other paralogs have not been described. The top DEGs between T4/T5 subtypes are side-IV (specific to T4c/T5c) and side-II (specific to T4d/T5d). LLPC2 and LLPC3 neurons express interacting Beats in a matching fashion; beat-Ia and beat-Ib are specific to LLPC2,

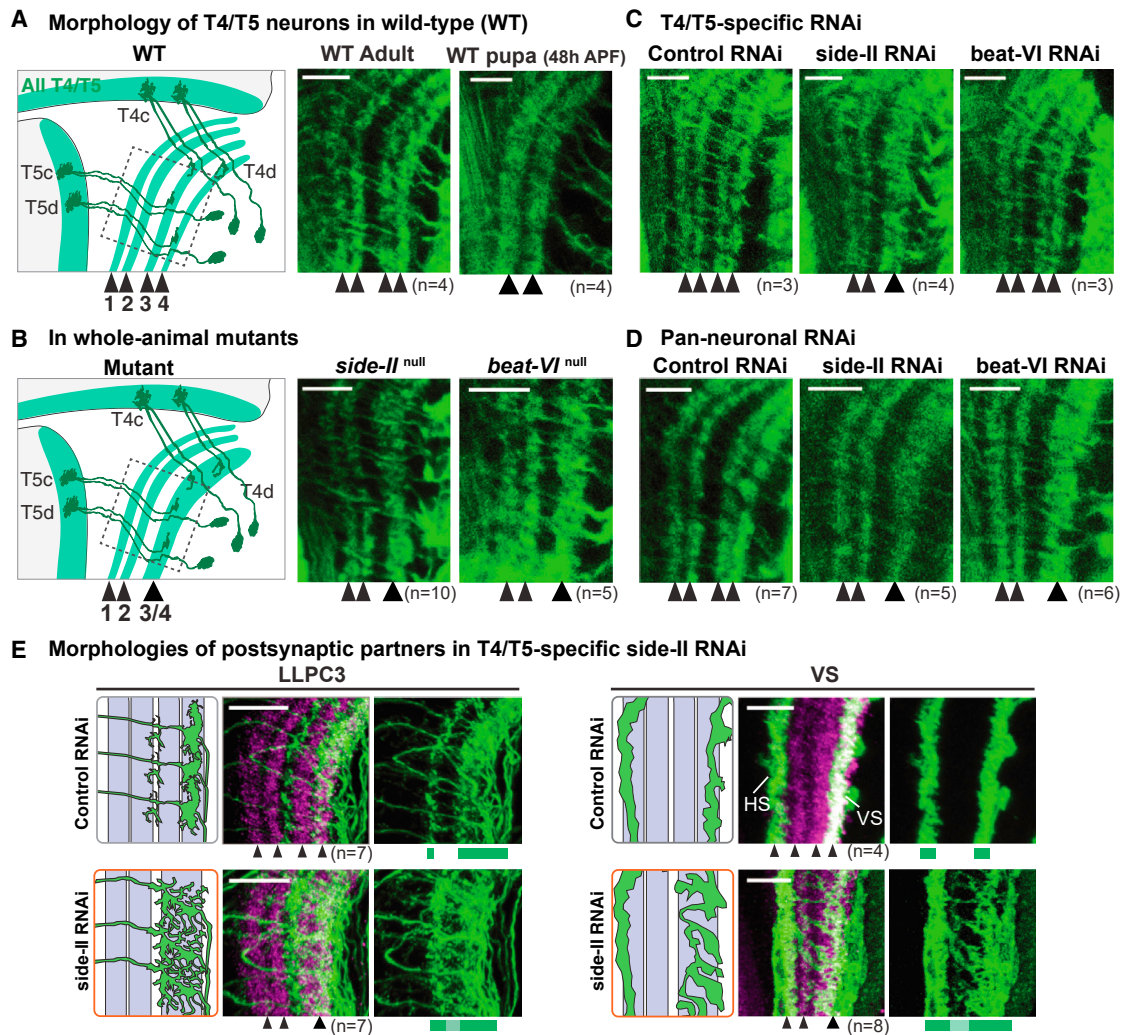


Figure 3. Side-II/Beat-VI receptor-ligand pair is required for the assembly of layers in the lobula plate

(A–D) Morphology of T4/T5s in the wild-type and mutant backgrounds. In immunofluorescence images, all T4/T5 neurons are labeled.

(A) During development (right), axon terminals first laminate into two broad domains (Lop1/2 and Lop3/4). In adults (middle), these layers further separate into four layers (Lop1/2/3/4).

(B) In *side-II*^{null} and *beat-VI*^{null} mutants, axons of T4c/T5c and T4d/T5d form a single fused Lop3/4 layer.

(C) T4/T5-specific RNAi of side-II (but not beat-VI) also results in fused Lop3/4.

(D) Pan-neuronal RNAi of both side-II and beat-VI results in fused Lop3/4.

(E) Morphology of the main postsynaptic partners of T4/T5s (green) upon removal of side-II from T4/T5s (via RNAi). In controls, LLPC3 and VS arborize in Lop4. In side-II RNAi, they span fused Lop3/4 layer. Phenotypes were observed in all samples. The sample size for each genotype is indicated under panels (n). Neuropil marker (magenta), Brp. Scale bars, 10 μ m.

See also Figure S3 and Table S1.

and beat-VI is specific to LLPC3 (Figure 2G). At least two other major synaptic targets of T4c/T5c (LPC2 and LPI3-4) express beat-IIa/IIb but not beat-VI, and the main synaptic target of T4d/T5d (VS) expresses beat-VI but not beat-IIb (Figures 2G and 2H). In this way, the matching expression of two pairs of interacting IgSF CAMs correlates with synaptic specificity in this circuitry (Figure 2J). As most neuron types in the developing visual system express one or more of the 14 Beat and 8 Side proteins and the expression of these cognate ligand/receptor pair matches between many synaptic partners these proteins may contribute to synaptic specificity more broadly (Figure S2).

The Side-II/Beat-VI receptor-ligand pair is required for the assembly of layers in the lobula plate

We sought to assess the roles of Beat/Side interactions in the wiring of T4/T5 axons. In wild type (WT), these axon terminals form four layers in the lobula plate (Figure 3A). In homozygous *side-II*^{null} mutant animals, T4/T5 axon terminals formed a single fused Lop3/4 layer (Figure 3B). Lop1 and Lop2 were normal. Beat-VI is a high-affinity binding partner of Side-II. Homozygous *beat-VI*^{null} mutants phenocopy *side-II*^{null} mutants. These results were confirmed with an insertion and a deletion disrupting these genes (Figures S3A and S3B). Both phenotypes were 100%

penetrant and observed in all examined samples (*side-II*^{null}, n = 10; *beat-VI*^{null}, n = 5). These implicate Side-II and Beat-VI in the same developmental process.

We then set out to determine which cell types require Side-II and Beat-VI for layer segregation. Removing side-II specifically from T4/T5s using RNA interference (RNAi) phenocopied *side-II*^{null} mutants (Figures 3C and 3D). These results were confirmed using an independent side-II RNAi line (Figure S3A). Removal of side-II from T4/T5s also disrupted dendritic morphologies of their main postsynaptic partners (Figure 3E). By contrast, removing beat-VI from T4/T5s did not result in the fusion of Lop3/4, whereas a pan-neuronal RNAi of beat-VI did (Figures 3C and 3D). All RNAi phenotypes were also 100% penetrant (see Figure 3 for sample sizes). The layer fusion phenotype resembles an early stage of lobula plate development in which the axons and dendrites of Lop3 and Lop4 form a single layer (Figure 3A). Thus, Side-II is required in T4d/T5d neurons and Beat-VI is required in other neurons (including their synaptic partners, see below) for the segregation of processes of synaptic partners into the same layer of lobula plate.

Matching expression patterns of Side-IV and Beat-IIa/IIb in Lop3 neurons suggested a similar role for this receptor-ligand pair in lobula plate development. However, in homozygous *side-IV*^{null} mutant animals, we did not observe defects in the lamination of T4/T5 axon terminals (Figure S3C). This suggests that these proteins have a different function, redundant pathways act in parallel, or that the lamination of Lop3/4 layers is driven predominantly by neurons targeting Lop4. A recent study has shown that Side-IV/Beat-IIb interactions can regulate wiring of other circuits of the visual system.²²

Side-II/Beat-VI restrict presynaptic sites and postsynaptic dendrites of synaptic partners to the same layer

We sought to assess the role of Side-II/Beat-VI interactions at the level of single cells in genetically mosaic animals. For T4/T5 neurons, we visualized the morphologies and distribution of presynaptic marker Brp of sparsely distributed homozygous *side-II*^{null} mutant neurons (see STAR Methods, Figures 4A–4C). WT T4c/T5c and T4d/T5d have presynaptic sites in Lop3 and Lop4, respectively. Mutant T4c/T5c were indistinguishable from WT. By contrast, although mutant T4d/T5d axons still terminate in Lop4, their presynaptic sites (Brp puncta) accumulate in both layers. This phenotype was seen in all mutant T4d/T5d neurons (n = 17, Figure 4G).

We next removed Beat-VI from postsynaptic partners, LLPC2 and LLPC3, using RNAi and visualized individual mutant neurons (see STAR Methods and Figures 4E and 4F). In controls, we detected WT LLPC2 (dendrites in Lop3) and LLPC3 (dendrites in Lop4). In beat-VI RNAi, we detected WT LLPC2 and many abnormal neurons spanning both Lop3 and Lop4. Fewer WT LLPC3s than expected were observed (Figure 4H, Fisher's exact test, p < 0.01). As beat-VI is expressed only in LLPC3 (not in LLPC2), we conclude that abnormal neurons are mutant LLPC3s. This phenotype was confirmed using an independent beat-VI RNAi line (Figure S4B). Dendritic branches of beat-VI-mutant LLPC3 neurons extending into Lop3 also contain ectopic postsynaptic markers as determined by cell-type-specific tagging of acetylcholine receptors (Sanfilippo, J.Y., and S.L.Z.,

unpublished data; Figure S4C). This is consistent with cholinergic T4/T5 neurons forming synapses with LLPC3 dendrites in Lop3.

The single-cell phenotypes of Side-II and Beat-VI are consistent with each other. That is, presynaptic sites of side-II mutant T4d/T5d and postsynaptic dendrites of beat-VI-deficient LLPC3 are no longer restricted to Lop4 and also accumulate in Lop3. These morphological changes may arise in different ways. Synaptic specificities of mutant neurons remain unaltered. In this scenario, mutations only affect the segregation of synapses to Lop4, and displaced presynaptic sites and postsynaptic dendrites in Lop3 still form connections with canonical synaptic partners.²³ Alternatively, mutant neurons may lose the ability to recognize with high fidelity their canonical synaptic partners and form connections with inappropriate targets. In this scenario, the removal of Side-II/Beat-VI interactions diminishes the molecular differences between correct and incorrect targets and they become less distinct. For instance, without Side-II, LLPC2, and LLPC3 appear more similar to T4d/T5d presynaptic terminals than in WT and they could form connections with both cell types (Figure 4I). This could explain why mutant T4d/T5d neurons form ectopic synapses in Lop3 and Lop4 but not in other layers of the lobula plate. This scenario is also consistent with the notion that synaptic specificity is determined by a hierarchy of wiring decisions sequentially restricting the pool of possible targets.^{24–26} Given the strong correlation between expression patterns of side-II and beat-VI, and synaptic specificities in this circuitry, we favor the second model (Figure 4I).

Regardless of mechanistic details, Side-II/Beat-VI interactions play a critical role in circuit assembly in Lop4. These proteins can promote adhesion between developing synaptic partners, leading to their segregation into a distinct layer where they form highly selective synaptic connections. The lack of separate genetic drivers for individual T4/T5 and LLPC subtypes currently limits our ability to directly assess changes in the synaptic connectivity of mutant neurons. Dense connectome reconstructions of mutant animals at the EM level, in future studies, will clarify the role of Side/Beat interactions in synaptic specificity.

Concluding remarks

Coupled transcriptome-connectome maps provide a description of gene expression patterns for both sides of synaptic connections. These maps can be correlated with binding specificities of cell surface proteins to chart possible molecular interactions between neurons. As more connectomes and developmental transcriptomes become available,^{2,27} comparative studies of highly related groups of neurons with divergent wiring specificities may prove fruitful in uncovering determinants of brain wiring in the mammalian brain. The remaining challenge in this field is the development of approaches for the rapid reconstruction of synaptic connectomes between the same neuron types in multiple animals of the same and different genetic backgrounds. Advances in expansion microscopy and genetic tools for cell-type-specific labeling of synaptic connections may provide scalable alternatives to EM-based connectomics.^{28–34}

The work described here expands the diverse repertoire of families of IgSF proteins that contribute to brain wiring in the *Drosophila* brain, e.g., Millard et al.³⁵ and Xu et al.³⁶ Each family forms complex receptor-ligand networks, including homophilic

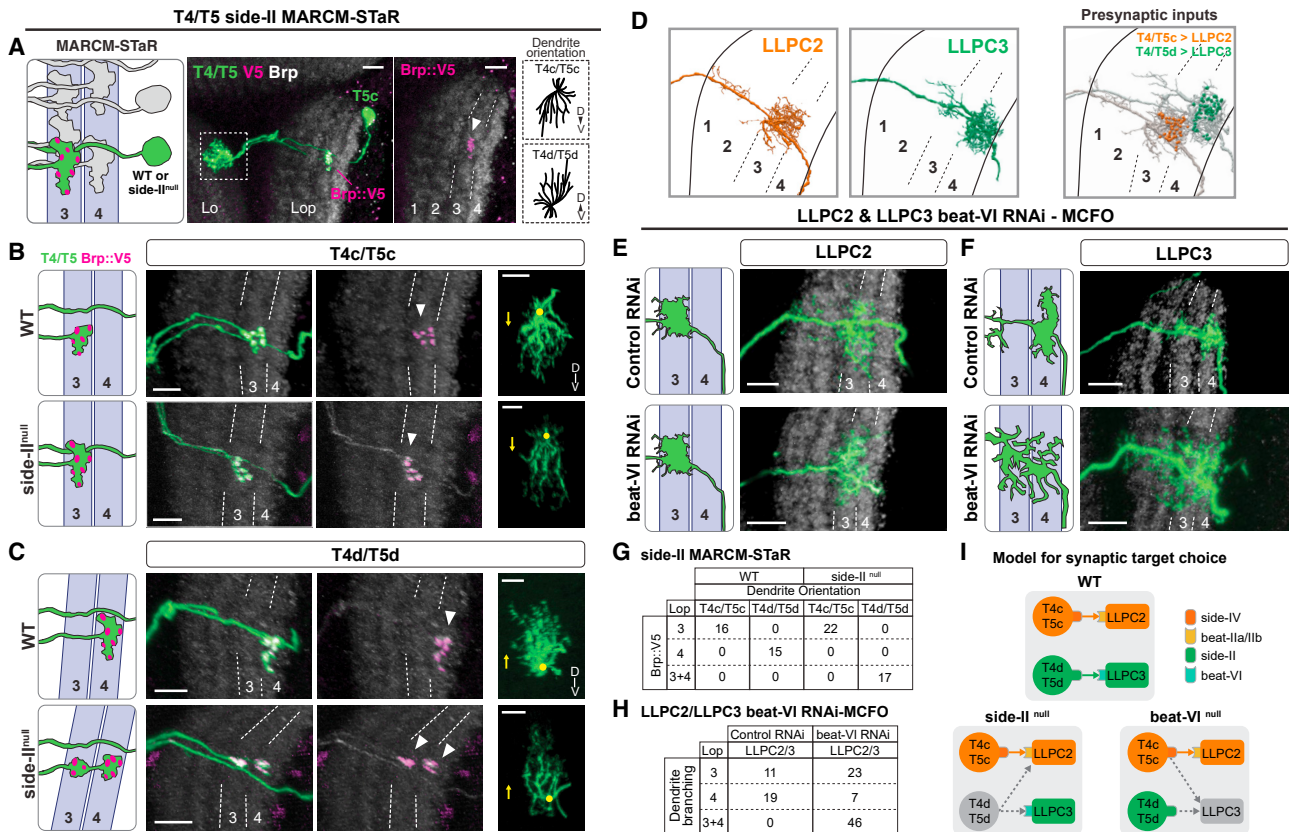


Figure 4. Side-II/Beat-VI restrict presynaptic sites and postsynaptic dendrites of synaptic partners to the same layer

(A–C) MARCM-STaR. Mosaics with homozygous mutant (*side-II^{null}*) T4/T5 neurons (green) with presynaptic marker Brp-V5 (magenta), and wild-type (WT) controls. (left) Schematics of T4/T5 axon terminals in Lop3 and Lop4. (right) Dendrite orientation discriminates between T4c/T5c and T4d/T5d (D, dorsal; V, ventral, based on the visual field coordinates).

(B) WT and *side-II^{null}* T4c/T5c form synapses in Lop3.

(C) WT T4d/T5d form synapses in Lop4; *side-II^{null}* T4d/T5d form synapses in Lop3 and Lop4.

(D) LLPC2 and LLPC3 morphologies and T4/T5 inputs from EM reconstruction.¹²

(E and F) *beat-VI* RNAi in LLPC2 and LLPC3. Single neurons were visualized using MCFO. In controls, both LLPC2 and LLPC3 dendrites were wild type (as in D). In *beat-VI* RNAi, we detected wild-type LLPC2 and fewer LLPC3 than expected. We observed a large number of abnormal neurons spanning both Lop3 and Lop4. As *beat-VI* is specific to LLPC3, we conclude that abnormal neurons are LLPC3.

(G) Quantification of the labeled neurons from (B) and (C).

(H) Quantifications of labeled neurons from (E) and (F).

(I) A hypothetical model of circuit rewiring upon removal of Side-II and Beat-VI from individual T4d/T5d and LLPC3 neurons in mosaics (see main text for discussion). Neuropil marker (gray), Brp. Scale bars, 10 μ m.

See also Figure S4 and Table S1.

(e.g., Dscams³⁷ thousands of isoforms) and heterophilic interactions (e.g., DIP/Dpr^{13,38} and Side/Beat⁶ comprising 50+ interacting pairs). These proteins are expressed in highly dynamic and cell-type-specific ways and with other cell surface proteins endowing each neuron with a unique cell surface protein composition.^{7,39} The logic in wiring the mammalian brain may be similar, with an expanded cadherin superfamily largely taking the place of IgSF diversity.^{10,40,41}

STAR★METHODS

Detailed methods are provided in the online version of this paper and include the following:

● KEY RESOURCES TABLE

● RESOURCE AVAILABILITY

- Lead contact
- Materials availability
- Data and code availability

● EXPERIMENTAL MODEL DETAILS

- Fly husbandry and genetics

● METHOD DETAILS

- Connectome analysis
- Transcriptome analysis
- Generation of null alleles using CRISPR
- MARCM-STaR experiment
- RNAi-MCFO experiment
- MCFO images for anatomy
- Cell-type specific labeling of acetylcholine receptor subunits in single neurons

- Immunohistochemistry for confocal microscopy
- Antibody information
- Tissue clearing and DPX mounting
- Confocal microscopy

SUPPLEMENTAL INFORMATION

Supplemental information can be found online at <https://doi.org/10.1016/j.cub.2023.08.020>.

ACKNOWLEDGMENTS

We thank Kazunori Shinomiya for sharing connectome data prior to publication. Stocks obtained from the Bloomington Drosophila Stock Center (NIH P40OD018537) and Vienna Drosophila Resource Center were used in this study. We also thank G.M. Rubin, H.J. Bellen, Qi Xiao, and Piero Sanfilippo for the reagents and the Janelia FlyLight Project Team for assistance with split-GAL4 screening and imaging. We thank members of the Zipursky lab for the critical discussion of the manuscript. S.L.Z. is an investigator of the Howard Hughes Medical Institute.

AUTHOR CONTRIBUTIONS

Conceptualization, J.Y., A.N., S.L.Z., and Y.Z.K.; investigation and formal analysis, J.Y., M.D., P.M., A.N., S.A.L., and Y.Z.K.; writing, J.Y., S.L.Z., and Y.Z.K.

DECLARATION OF INTERESTS

The authors declare no competing interests.

Received: March 27, 2023

Revised: July 12, 2023

Accepted: August 4, 2023

Published: August 29, 2023

REFERENCES

1. Zheng, Z., Lauritzen, J.S., Perlman, E., Robinson, C.G., Nichols, M., Milkie, D., Torrens, O., Price, J., Fisher, C.B., Sharifi, N., et al. (2018). A complete electron microscopy volume of the brain of adult *Drosophila melanogaster*. *Cell* 174, 730–743.e22. <https://doi.org/10.1016/j.cell.2018.06.019>.
2. Scheffer, L.K., and Meinertzhagen, I.A. (2019). The fly brain atlas. *Annu. Rev. Cell Dev. Biol.* 35, 637–653. <https://doi.org/10.1146/annurev-cell-bio-100818-125444>.
3. Motta, A., Berning, M., Boergens, K.M., Staffler, B., Beining, M., Loomba, S., Hennig, P., Wissler, H., and Helmstaedter, M. (2019). Dense connectomic reconstruction in layer 4 of the somatosensory cortex. *Science* 366, eaay3134. <https://doi.org/10.1126/science.aay3134>.
4. Scheffer, L.K., Xu, C.S., Januszewski, M., Lu, Z., Takemura, S.Y., Hayworth, K.J., Huang, G.B., Shinomiya, K., Maitlin-Shepard, J., Berg, S., et al. (2020). A connectome and analysis of the adult *Drosophila* central brain. *eLife* 9, e57443. <https://doi.org/10.7554/eLife.57443>.
5. Dorkenwald, S., Turner, N.L., Macrina, T., Lee, K., Lu, R., Wu, J., Bodor, A.L., Bleckert, A.A., Brittain, D., Kemnitz, N., et al. (2022). Binary and analog variation of synapses between cortical pyramidal neurons. *eLife* 11, e76120. <https://doi.org/10.7554/eLife.76120>.
6. Li, H., Watson, A., Olechwiec, A., Anaya, M., Sorooshiyari, S.K., Harnett, D.P., Lee, H.-K.P., Vielmetter, J., Fares, M.A., Garcia, K.C., et al. (2017). Deconstruction of the beaten Path-Sidestep interaction network provides insights into neuromuscular system development. *eLife* 6, 270. <https://doi.org/10.7554/eLife.28111>.
7. Kurmangaliyev, Y.Z., Yoo, J., Valdes-Aleman, J., Sanfilippo, P., and Zipursky, S.L. (2020). Transcriptional programs of circuit assembly in the *Drosophila* visual system. *Neuron* 108, 1045–1057.e6. <https://doi.org/10.1016/j.neuron.2020.10.006>.
8. Özel, M.N., Simon, F., Jafari, S., Holguera, I., Chen, Y.-C., Benhra, N., El-Danaf, R.N., Kapuralin, K., Malin, J.A., Konstantinides, N., et al. (2021). Neuronal diversity and convergence in a visual system developmental atlas. *Nature* 589, 88–95. <https://doi.org/10.1038/s41586-020-2879-3>.
9. Südhof, T.C. (2021). The cell biology of synapse formation. *J. Cell Biol.* 220, e202103052. <https://doi.org/10.1083/jcb.202103052>.
10. Sanes, J.R., and Zipursky, S.L. (2020). Synaptic specificity, recognition molecules, and assembly of neural circuits. *Cell* 181, 536–556. <https://doi.org/10.1016/j.cell.2020.04.008>.
11. Shinomiya, K., Huang, G., Lu, Z., Parag, T., Xu, C.S., Aniceto, R., Ansari, N., Cheatham, N., Lauchie, S., Neace, E., et al. (2019). Comparisons between the ON- and OFF-edge motion pathways in the *Drosophila* brain. *eLife* 8, e40025. <https://doi.org/10.7554/eLife.40025>.
12. Shinomiya, K., Nern, A., Meinertzhagen, I.A., Plaza, S.M., and Reiser, M.B. (2022). Neuronal circuits integrating visual motion information in *Drosophila melanogaster*. *Curr. Biol.* 32, 3529–3544.e2. <https://doi.org/10.1016/j.cub.2022.06.061>.
13. Özkan, E., Carrillo, R.A., Eastman, C.L., Weiszmann, R., Waghray, D., Johnson, K.G., Zinn, K., Celniker, S.E., and Garcia, K.C. (2013). An extracellular interactome of immunoglobulin and LRR proteins reveals receptor-ligand networks. *Cell* 154, 228–239. <https://doi.org/10.1016/j.cell.2013.06.006>.
14. Borst, A., Haag, J., and Mauss, A.S. (2020). How fly neurons compute the direction of visual motion. *J. Comp. Physiol. A Neuroethol. Sens. Neural Behav. Physiol.* 206, 109–124. <https://doi.org/10.1007/s00359-019-01375-9>.
15. Maisak, M.S., Haag, J., Ammer, G., Serbe, E., Meier, M., Leonhardt, A., Schilling, T., Bahl, A., Rubin, G.M., Nern, A., et al. (2013). A directional tuning map of *Drosophila* elementary motion detectors. *Nature* 500, 212–216. <https://doi.org/10.1038/nature12320>.
16. Kurmangaliyev, Y.Z., Yoo, J., LoCascio, S.A., and Zipursky, S.L. (2019). Modular transcriptional programs separately define axon and dendrite connectivity. *eLife* 8, 505. <https://doi.org/10.7554/eLife.50822>.
17. Davis, F.P., Nern, A., Picard, S., Reiser, M.B., Rubin, G.M., Eddy, S.R., and Henry, G.L. (2020). A genetic, genomic, and computational resource for exploring neural circuit function. *eLife* 9, e50901. <https://doi.org/10.7554/eLife.50901>.
18. Isaacson, M.D., Eliason, J.L.M., Nern, A., Rogers, E.M., Lott, G.K., Tabachnik, T., Rowell, W.J., Edwards, A.W., Korff, W.L., Rubin, G.M., et al. (2023). Small-field visual projection neurons detect translational optic flow and support walking control. <https://doi.org/10.1101/2023.06.21.546024>.
19. Fambrough, D., and Goodman, C.S. (1996). The *Drosophila* beaten path Gene Encodes a Novel Secreted Protein That Regulates Defasciculation at Motor Axon Choice Points. *Cell* 87, 1049–1058. [https://doi.org/10.1016/s0092-8674\(00\)81799-7](https://doi.org/10.1016/s0092-8674(00)81799-7).
20. Sink, H., Rehm, E.J., Richstone, L., Bulls, Y.M., and Goodman, C.S. (2001). sidestep encodes a target-derived attractant essential for motor axon guidance in *Drosophila*. *Cell* 105, 57–67. [https://doi.org/10.1016/s0092-8674\(01\)00296-3](https://doi.org/10.1016/s0092-8674(01)00296-3).
21. Siebert, M., Banovic, D., Goellner, B., and Aberle, H. (2009). *Drosophila* motor axons recognize and follow a Sidestep-labeled substrate pathway to reach their target fields. *Genes Dev.* 23, 1052–1062. <https://doi.org/10.1101/gad.520509>.
22. Osaka, J., Ishii, A., Wang, X., Hakeda-Suzuki, S., Iwanaga, R., Kawamura, H., and Suzuki, T. (2023). Complex formation of immunoglobulin superfamily molecules side-IV and beat-11b regulates synaptic specificity in the *Drosophila* visual system. <https://doi.org/10.1101/2023.03.27.534487>.
23. Valdes-Aleman, J., Fetter, R.D., Sales, E.C., Heckman, E.L., Venkatasubramanian, L., Doe, C.Q., Landgraf, M., Cardona, A., and Zlatic, M. (2021). Comparative connectomics reveals how partner identity, location, and activity specify synaptic connectivity in *Drosophila*. *Neuron* 109, 105–122.e7. <https://doi.org/10.1016/j.neuron.2020.10.004>.

24. Kolodkin, A.L., and Hiesinger, P.R. (2017). Wiring visual systems: common and divergent mechanisms and principles. *Curr. Opin. Neurobiol.* **42**, 128–135. <https://doi.org/10.1016/j.conb.2016.12.006>.
25. Xu, C., Theisen, E., Maloney, R., Peng, J., Santiago, I., Yapp, C., Werkhoven, Z., Rumbaut, E., Shum, B., Tarnogorska, D., et al. (2019). Control of synaptic specificity by establishing a relative preference for synaptic partners. *Neuron* **103**, 865–877.e7. <https://doi.org/10.1016/j.neuron.2019.06.006>.
26. Zhang, C., Hellevik, A., Takeuchi, S., and Wong, R.O. (2022). Hierarchical partner selection shapes rod-cone pathway specificity in the inner retina. *Iscience* **25**, 105032. <https://doi.org/10.1016/j.isci.2022.105032>.
27. Zeng, H. (2022). What is a cell type and how to define it? *Cell* **185**, 2739–2755. <https://doi.org/10.1016/j.cell.2022.06.031>.
28. Tillberg, P.W., Chen, F., Piatkevich, K.D., Zhao, Y., Yu, C.-C.J., English, B.P., Gao, L., Martorell, A., Suk, H.-J., Yoshida, F., et al. (2016). Protein-retention expansion microscopy of cells and tissues labeled using standard fluorescent proteins and antibodies. *Nat. Biotechnol.* **34**, 987–992. <https://doi.org/10.1038/nbt.3625>.
29. Gao, Y., Hisey, E., Bradshaw, T.W.A., Erata, E., Brown, W.E., Courtland, J.L., Uezu, A., Xiang, Y., Diau, Y., and Soderling, S.H. (2019). Plug-and-play protein modification using homology-independent universal genome engineering. *Neuron* **103**, 583–597.e8. <https://doi.org/10.1016/j.neuron.2019.05.047>.
30. Chen, Y., Akin, O., Nern, A., Tsui, C.Y.K., Pecot, M.Y., and Zipursky, S.L. (2014). Cell-type-specific labeling of synapses in vivo through synaptic tagging with recombination. *Neuron* **81**, 280–293. <https://doi.org/10.1016/j.neuron.2013.12.021>.
31. Fendl, S., Vieira, R.M., and Borst, A. (2020). Conditional protein tagging methods reveal highly specific subcellular distribution of ion channels in motion-sensing neurons. *eLife* **9**, 2247–2226. <https://doi.org/10.7554/eLife.62953>.
32. Lillvis, J.L., Otsuna, H., Ding, X., Pisarev, I., Kawase, T., Colonell, J., Rokicki, K., Goina, C., Gao, R., Hu, A., et al. (2022). Rapid reconstruction of neural circuits using tissue expansion and light sheet microscopy. *eLife* **11**, e81248. <https://doi.org/10.7554/eLife.81248>.
33. Parisi, M.J., Aimino, M.A., and Mosca, T.J. (2023). A conditional strategy for cell-type-specific labeling of endogenous excitatory synapses in *Drosophila*. *Cell Rep. Methods* **3**, 100477. <https://doi.org/10.1016/j.crmeth.2023.100477>.
34. Bourke, A.M., Bowen, A.B., and Kennedy, M.J. (2018). New approaches for solving old problems in neuronal protein trafficking. *Mol. Cell. Neurosci.* **91**, 48–66. <https://doi.org/10.1016/j.mcn.2018.04.004>.
35. Millard, S.S., Lu, Z., Zipursky, S.L., and Meinertzhagen, I.A. (2010). *Drosophila* dscam proteins regulate postsynaptic specificity at multiple-contact synapses. *Neuron* **67**, 761–768. <https://doi.org/10.1016/j.neuron.2010.08.030>.
36. Xu, S., Xiao, Q., Cosmanescu, F., Sergeeva, A.P., Yoo, J., Lin, Y., Katsamba, P.S., Ahlsen, G., Kaufman, J., Linaval, N.T., et al. (2018). Interactions between the Ig-superfamily proteins DIP- α and Dpr6/10 regulate assembly of neural circuits. *Neuron* **100**, 1369–1384.e6. <https://doi.org/10.1016/j.neuron.2018.11.001>.
37. Wojtowicz, W.M., Wu, W., Andre, I., Qian, B., Baker, D., and Zipursky, S.L. (2007). A vast repertoire of Dscam binding specificities arises from modular interactions of variable Ig domains. *Cell* **130**, 1134–1145. <https://doi.org/10.1016/j.cell.2007.08.026>.
38. Cosmanescu, F., Katsamba, P.S., Sergeeva, A.P., Ahlsen, G., Patel, S.D., Brewer, J.J., Tan, L., Xu, S., Xiao, Q., Nagarkar-Jaiswal, S., et al. (2018). Neuron-subtype-specific expression, interaction affinities, and specificity determinants of DIP/Dpr cell recognition proteins. *Neuron* **100**, 1385–1400.e6. <https://doi.org/10.1016/j.neuron.2018.10.046>.
39. Sperry, R.W. (1963). Chemoaffinity in the orderly growth of nerve fiber patterns and connections. *Proc. Natl. Acad. Sci. USA* **50**, 703–710. <https://doi.org/10.1073/pnas.50.4.703>.
40. Duan, X., Krishnaswamy, A., Laboulaye, M.A., Liu, J., Peng, Y.-R., Yamagata, M., Toma, K., and Sanes, J.R. (2018). Cadherin combinations recruit dendrites of distinct retinal neurons to a shared interneuronal scaffold. *Neuron* **99**, 1145–1154.e6. <https://doi.org/10.1016/j.neuron.2018.08.019>.
41. Canzio, D., and Maniatis, T. (2019). The generation of a protocadherin cell-surface recognition code for neural circuit assembly. *Curr. Opin. Neurobiol.* **59**, 213–220. <https://doi.org/10.1016/j.conb.2019.10.001>.
42. Fujiwara, T., Cruz, T.L., Bohnslav, J.P., and Chiappe, M.E. (2017). A faithful internal representation of walking movements in the *Drosophila* visual system. *Nat. Neurosci.* **20**, 72–81. <https://doi.org/10.1038/nn.4435>.
43. Klapoetke, N.C., Nern, A., Peek, M.Y., Rogers, E.M., Breads, P., Rubin, G.M., Reiser, M.B., and Card, G.M. (2017). Ultra-selective looming detection from radial motion opponency. *Nature* **551**, 237–241. <https://doi.org/10.1038/nature24626>.
44. Nern, A., Pfeiffer, B.D., and Rubin, G.M. (2015). Optimized tools for multi-color stochastic labeling reveal diverse stereotyped cell arrangements in the fly visual system. *Proc. Natl. Acad. Sci. USA* **112**, E2967–E2976. <https://doi.org/10.1073/pnas.1506763112>.
45. Butler, A., Hoffman, P., Smibert, P., Papalexis, E., and Satija, R. (2018). Integrating single-cell transcriptomic data across different conditions, technologies, and species. *Nat. Biotechnol.* **36**, 411–420. <https://doi.org/10.1038/nbt.4096>.
46. Bates, A.S., Manton, J.D., Jagannathan, S.R., Costa, M., Schlegel, P., Rohlfing, T., and Jefferis, G.S. (2020). The natverse, a versatile toolbox for combining and analysing neuroanatomical data. *eLife* **9**, e53350. <https://doi.org/10.7554/eLife.53350>.
47. Shannon, P., Markiel, A., Ozier, O., Baliga, N.S., Wang, J.T., Ramage, D., Amin, N., Schwikowski, B., and Ideker, T. (2003). Cytoscape: A software environment for integrated models of biomolecular interaction networks. *Genome Res.* **13**, 2498–2504. <https://doi.org/10.1101/gr.1239303>.
48. Csardi, G., and Nepusz, T. (2006). The igraph software package for complex network research. *InterJournal, Complex Syst.* **1695**, 1–9.
49. Clements, J., Dolafi, T., Umayam, L., Neubarth, N.L., Berg, S., Scheffer, L.K., and Plaza, S.M. (2020). neuPrint: analysis tools for EM connectomics. <https://doi.org/10.1101/2020.01.16.909465>.
50. Pei, J., Kinch, L.N., and Grishin, N.V. (2018). FlyXCDB—A resource for *Drosophila* cell surface and secreted proteins and their extracellular domains. *J. Mol. Biol.* **430**, 3353–3411. <https://doi.org/10.1016/j.jmb.2018.06.002>.
51. Murtagh, F., and Legendre, P. (2014). Ward’s hierarchical agglomerative clustering method: which algorithms implement Ward’s criterion? *J. Classif.* **31**, 274–295. <https://doi.org/10.1007/s00357-014-9161-z>.
52. Paradis, E., and Schliep, K. (2019). ape 5.0: an environment for modern phylogenetics and evolutionary analyses in R. *Bioinformatics* **35**, 526–528. <https://doi.org/10.1093/bioinformatics/bty633>.
53. Ren, X., Sun, J., Housden, B.E., Hu, Y., Roesel, C., Lin, S., Liu, L.-P., Yang, Z., Mao, D., Sun, L., et al. (2013). Optimized gene editing technology for *Drosophila melanogaster* using germ line-specific Cas9. *Proc. Natl. Acad. Sci. USA* **110**, 19012–19017. <https://doi.org/10.1073/pnas.1318481110>.
54. Lee, T., and Luo, L. (2001). Mosaic analysis with a repressible cell marker (MARCM) for *Drosophila* neural development. *Trends Neurosci.* **24**, 251–254.

STAR★METHODS

KEY RESOURCES TABLE

REAGENT or RESOURCE	SOURCE	IDENTIFIER
Antibodies		
chicken anti-GFP	Abcam	Cat# ab13970; RRID:AB_300798
rabbit anti-DsRed	Takara Bio	Cat# 632496; RRID:AB_10013483
mouse anti-Nc82	Developmental Studies Hybridoma Bank (DSHB)	Cat# nc82; RRID:AB_2314866
chicken anti-V5	Bethyl	Cat# A190-118A; RRID:AB_66741
rabbit anti-HA	Cell Signaling Technology	Cat# 3724; RRID:AB_1549585
guinea pig anti-Pdm3	a gift from John Carlson	N/A
mouse anti-Br	Developmental Studies Hybridoma Bank (DSHB)	Cat# Broad-core (25E9.D7); RRID:AB_528104
rabbit anti-Ollas	GenScript	Cat# A01658; RRID:AB_2622186
goat anti-chicken Alexa Fluor 488	Thermo Fisher Scientific	Cat# A-11039; RRID:AB_2534096
goat anti-rabbit AF568	Thermo Fisher Scientific	Cat# A-11011; RRID:AB_143157
goat anti-guinea pig AF568	Thermo Fisher Scientific	Cat# A-11075; RRID:AB_2534119
goat anti-mouse AF568	Thermo Fisher Scientific	Cat# A-11031; RRID:AB_144696
goat anti-mouse AF647	Thermo Fisher Scientific	Cat# A-21235; RRID:AB_2535804
FluoTag-X4 anti-rabbit AbberiorStar635P	NanoTag Biotechnologies	Cat# N2404-Ab635P
Chemicals, peptides, and recombinant proteins		
Xylene	Fisher Scientific	Cat#X5-500
DPX	Electron Microscopy Sciences	Cat#13510
Deposited data		
Connectome of the lobula plate	Shinomiya et al. ¹¹ ; Shinomiya et al. ¹²	https://neuprint.janelia.org (Fib19:V1.0)
Single-cell transcriptional atlas of the <i>Drosophila</i> visual system (V1.0)	Kurmangaliyev et al. ⁷	https://doi.org/10.5281/zenodo.8097374
Single-cell transcriptional atlas of the <i>Drosophila</i> visual system (V1.1)	This study	https://doi.org/10.5281/zenodo.8111612
Experimental models: Organisms/strains		
<i>D. melanogaster</i> : w[1118]; PBac[y+mDint2] w[+mC]=UAS-CD4-tdTom)VK00033	Bloomington <i>Drosophila</i> Stock Center	BDSC:35837
<i>D. melanogaster</i> : w[1118]; P{y[+t7.7] w[+mC]=GMR42F06-GAL4}attP2	Bloomington <i>Drosophila</i> Stock Center	BDSC:41253
<i>D. melanogaster</i> : w[1118]; P{y[+t7.7] w[+mC]=GMR39E01-lexA}attP40	Fujiwara et al. ⁴²	BDSC:52776
<i>D. melanogaster</i> : w[1118]; P{y[+t7.7] w[+mC]=GMR42F06-lexA}attP40	Bloomington <i>Drosophila</i> Stock Center	BDSC:54203
<i>D. melanogaster</i> : P{w[+mC]=UAS-Dcr-2.D}1, w[1118];+;+	Bloomington <i>Drosophila</i> Stock Center	BDSC:24646
<i>D. melanogaster</i> : y[1] w[*]; P{w[+mC]=UAS-CD4-tdGFP}8M2	Bloomington <i>Drosophila</i> Stock Center	BDSC:35839
<i>D. melanogaster</i> : w[1118]; P{y[+t7.7] w[+mC]=GMR23G12-GAL4}attP2	Bloomington <i>Drosophila</i> Stock Center	BDSC:49044
<i>D. melanogaster</i> : P{w[+mW.hs]=GawB}elav[C155]	Bloomington <i>Drosophila</i> Stock Center	BDSC:458
<i>D. melanogaster</i> : w[*]; P{y[+t7.7] w[+mC]=13XLexAop2-IVS-myr::GFP}attP2	Bloomington <i>Drosophila</i> Stock Center	BDSC:32209
<i>D. melanogaster</i> : w[1118]; P{y[+t7.7] w[+mC]=GMR21D07-lexA}attP40	Bloomington <i>Drosophila</i> Stock Center	BDSC:54637

(Continued on next page)

Continued

REAGENT or RESOURCE	SOURCE	IDENTIFIER
<i>D. melanogaster</i> : w[1118]; P{y[+7.7] w[+mC]=13XLexAop2-IVS-myr::GFP}su(Hw)attP1	Bloomington Drosophila Stock Center	BDSC:32212
<i>D. melanogaster</i> : y[1] w[*]; P{w[+mC]=tubP-GAL80}LL10 P{ry[+7.2]=neoFRT}40A/CyO	Bloomington Drosophila Stock Center	BDSC:5192
<i>D. melanogaster</i> : w[1118]; P{y[+7.7] w[+mC]=GMR42H07-GAL4}attP2	Bloomington Drosophila Stock Center	BDSC:50172
<i>D. melanogaster</i> : w[1118] P{y[+7.7] w[+mC]=hs-FLPG5.PEST}attP3	Bloomington Drosophila Stock Center	BDSC:62118
<i>D. melanogaster</i> : w[1118]; P{y[+7.7] w[+mC]=10xUAS(FRT.stop)myr::smGdP-V5-THS-10xUAS(FRT.stop)myr::smGdP-FLAG}su(Hw)attP5	Bloomington Drosophila Stock Center	BDSC:62124
<i>D. melanogaster</i> : w[*]; T1{FLP}fru[FLP]/TM3, Sb[1]	Bloomington Drosophila Stock Center	BDSC:66870
<i>D. melanogaster</i> : y[1] w[*]; T1{GFP[3xP3.cLa]=CRIMIC.TG4.0}dmrt99B[CR70107-TG4.0]	Bloomington Drosophila Stock Center	BDSC:92707
<i>D. melanogaster</i> : w[*]; P{y[+7.7] w[+mC]=10XUAS-IVS-myr::GFP}attP2	Bloomington Drosophila Stock Center	BDSC:32197
<i>D. melanogaster</i> : Deficiency for side-II; w[1118]; Df(2L)ED3, P{w[+mW.Scer\FRT.hs3]=3'.RS5+3.3'}ED3/SM6a	Bloomington Drosophila Stock Center	BDSC:6963
<i>D. melanogaster</i> : y[1] w[*]; Mi{y[+mDint2]=MIC}beat-VI[M113252]	Bloomington Drosophila Stock Center	BDSC:58680
<i>D. melanogaster</i> : w: 10XUAS-FSF-myrGFP-2A-KDR::Pest;+	Zipursky lab (Sanfilippo et al.)	N/A
<i>D. melanogaster</i> : w;nAChR α 5-smGdP-ollas;	Zipursky lab (Sanfilippo et al.)	N/A
<i>D. melanogaster</i> : w;nAChR α 6-smGdP-ollas;	Zipursky lab (Sanfilippo et al.)	N/A
<i>D. melanogaster</i> : w; R28D05-p65ADZp attP40; R55H05-ZpGdbd attP2	Klapoetke et al. ⁴³	SS00810
<i>D. melanogaster</i> : w; VT004319-p65ADZp attP40; VT044492-ZpGdbd attP2	This Study	SS02408
<i>D. melanogaster</i> : VT029598-p65ADZp attP40; 55H05-ZpGdbd attP2	This Study	SS02580
<i>D. melanogaster</i> : w; R81A05-p65ADZp attP40/CyO::Tb-RFP; VT043014-ZpGdbd attP2	Davis et al. ¹⁷	SS02700
<i>D. melanogaster</i> : VT032900-p65ADZ attP40; VT016114-ZpGdbd attP2	Isaacson et al. ¹⁸	SS25868
<i>D. melanogaster</i> : VT057342-p65ADZp attP40;VT044492-ZpGdbd attP2	Isaacson et al. ¹⁸	SS02407
<i>D. melanogaster</i> : VT029598-p65ADZp attP40; VT005006-ZpGdbd attP2	This Study	SS02440
<i>D. melanogaster</i> : P{VT046081-GAL4}attP2	Vienna Drosophila Resource Center	VDRC#207065
<i>D. melanogaster</i> : empty attP control line	Vienna Drosophila Resource Center	VDRC#TK-60100
<i>D. melanogaster</i> : UAS-RNAi of side-II: P{KK111520}VIE-260B	Vienna Drosophila Resource Center	VDRC#KK-107512
<i>D. melanogaster</i> : UAS-RNAi of side-II: P{KK114253}VIE-260B	Vienna Drosophila Resource Center	VDRC#KK-103687
<i>D. melanogaster</i> : UAS-RNAi of beat-VI: P{KK110930}VIE-260B	Vienna Drosophila Resource Center	VDRC #KK-105798
<i>D. melanogaster</i> : UAS-RNAi of beat-VI: w1118; P{GD89}v6694	Vienna Drosophila Resource Center	VDRC#GD-6694
<i>D. melanogaster</i> : UAS-RNAi of side-IV: P{KK111999}VIE-260B	Vienna Drosophila Resource Center	VDRC#KK-102563

(Continued on next page)

Continued

REAGENT or RESOURCE	SOURCE	IDENTIFIER
<i>D. melanogaster</i> : UAS-RNAi of side-IV: w1118; P{GD5643}v16636	Vienna Drosophila Resource Center	VDRC#GD-16636
<i>D. melanogaster</i> : w[1118] P{y[+7.7] w[+mC]=10xUAS-IVS-myr::smGdP-HA} attP18 P{y[+7.7] w[+mC]=13xLexAop2-IVS-myr::smGdP-V5}su(Hw)attP8; TM2/TM6B, Tb[1]	Rubin Lab; Nern et al. ⁴⁴	BDSC: 64092
<i>D. melanogaster</i> : DIP-beta-LexA;+;+	Zipursky Lab	DIP-beta-LexA
<i>D. melanogaster</i> : UAS-beat-VI.ORF.3xHA	FlyORF	F002906
<i>D. melanogaster</i> : side-II null allele. w;side-II[13];+	This paper	side-II[13]
<i>D. melanogaster</i> : side-IV null allele. w;Bl/CyO;side-IV[4-5]/TM6B	This paper	side-IV[4-5]
<i>D. melanogaster</i> : beat-VI null allele. w;Bl/CyO;beat-VI[4]/TM6B	This paper	beat-VI[4]
Software and algorithms		
Seurat V4.1.1	Butler et al. ⁴⁵	https://satijalab.org
Imaris 9	Oxford Instruments	https://imaris.oxinst.com
natverse 0.2.4	Bates et al. ⁴⁶	https://natverse.org
Cytoscape	Shannon et al. ⁴⁷	https://cytoscape.org
igraph	Csardi and Nepusz ⁴⁸	https://igraph.org
ImageJ (Fiji)	https://fiji.sc	N/A

RESOURCE AVAILABILITY

Lead contact

Further information and requests for resources and reagents should be directed to and will be fulfilled by the lead contact, Y.Z.K. (yerbol@brandeis.edu).

Materials availability

Newly generated mutant alleles and split-Gal4 fly lines are available upon request. Split-Gal4 lines are available via <https://splitgal4.janelia.org/cgi-bin/splitgal4.cgi>.

Data and code availability

Connectome datasets used in this study are available through Neuprint (neuprint.janelia.org): fib19:v1.0. Transcriptome datasets are available on Zenodo:8097374, 8111612 and NCBI GEO: GSE156455. The source code for the analysis is available on GitHub: https://github.com/kurmangaliyev-lab/Yoo_2023. Any additional information required to reanalyze the data reported in this paper is available from the [lead contact](#) upon request.

EXPERIMENTAL MODEL DETAILS

Fly husbandry and genetics

Flies were kept on standard cornmeal medium at 25°C, 12-hour light/dark cycles. All RNAi experiments were run with UAS-Dcr2.D. Detailed genotypes for all figures and [supplemental information](#) are included in [Table S1](#).

Split-GAL4 lines have been previously described^{17,18,43} or were newly constructed as described.^{17,18}

METHOD DETAILS

Connectome analysis

T4/T5 connectomes^{11,12} were downloaded from the neuPrint database (<https://neuprint.janelia.org/>, dataset: fib19:V1.0⁴⁹) using natverse (0.2.4) package.^{12,46} Synaptic connectivity data (inputs and outputs) were downloaded for 40 representative T4/T5 neurons from published data¹² (five instances of each T4/T5 subtype). For each representative neuron, we summed the total number of synapses between a given instance of T4/T5 and all synaptic partners of the same cell type (e.g. total number of synapses between a single T4a and any Mi1 neurons). This data was plotted as a heatmap of synaptic weights between partner neuron types and

individual instances of T4/T5 neurons (Figure 1B). Synaptic weights were averaged across all instances of each T4/T5 subtype to generate a cell type-level connectome graph. The connectome graph was visualized using Cytoscape⁴⁷ and igraph⁴⁸ (Figure 1A). Synaptic partners were restricted to cell types that make more than 10 synapses with a single T4/T5 neuron. Only connections with more than 7 synapses have been plotted. Presynaptic inputs were restricted to connections in the medulla and lobula; postsynaptic outputs were restricted to connections in the lobula plate. Reconstructions of representative LLPC2 and LLPC3 neurons in Figure 4D were visualized in neuPrint.

Transcriptome analysis

Analysis of the transcriptional atlas of the *Drosophila* visual system

Single-cell analysis was performed using Seurat (V4.1.1).⁴⁵ All functions were used with default parameters unless otherwise indicated. In this study, we use single-cell RNA-Seq data from a previously generated comprehensive transcriptional atlas of the developing visual system.⁷ We focus on the main dataset including samples from seven developmental time points taken every 12 hours from 24 to 96h APF. In the initial version of the visual system atlas (V1.0), 58 transcriptional clusters were matched to known morphological cell types. Two of these clusters were annotated as LLPC1 and LPC1 neurons based on correlation analysis with available bulk reference datasets.⁷ A more detailed evaluation of these clusters revealed further heterogeneity in the LLPC1 cluster. We subsetted and reclustered LLPC1 and LPC1 clusters separately from the rest of the dataset. This analysis was performed after the integration of the main dataset as previously described.⁷ After subsetting, a new set of 1000 highly variable genes was selected, scaled, and used for principal component analysis (functions: FindVariableFeatures, ScaleData, RunPCA). The first nine principal components were used for the generation of tSNE plots and clustering (functions: RunTSNE, FindNeighbors, FindClusters, resolution = 0.1). The analysis revealed five transcriptionally distinct clusters of LPC/LLPC neurons. Clusters were annotated based on the expression of cell-type-specific marker genes (Figure S1). Cell types of LPC/LLPC neurons were renamed in the main dataset of the visual system atlas (V1.1).

Visualization of gene expression patterns

Expression patterns of genes were visualized using average expression levels for each cell type and time point. Averaging was performed for each replicate in non-log space for the original normalized expression values (TP10K, transcripts-per-10,000). For the heatmaps, we used log_{1p}-transformed expression values averaged across replicates (capped at the maximum expression value of 20). For the line plots, we used expression values in linear scale. The list of all IgSF proteins was obtained from FlyXCDB (<http://prodata.swmed.edu/FlyXCDB>).⁵⁰

Hierarchical clustering of neuronal cell types

Clustering was performed for neuronal cell types from one sample at 48h APF (W1118 sample, replicate B). This analysis was performed based on the original normalized expression values (pre-integration). We selected 1000 highly variable genes and computed average expression levels for each cell type (functions: FindVariableFeatures, AverageExpression). Hierarchical clustering was performed based on Pearson's correlation coefficients between log-transformed expression profiles of each cell type (distance metric: 1 - Pearson's r; clustering method: ward.D2).⁵¹ Clustering results were visualized as a dendrogram (function: ape::plot.phylo).⁵²

Differential gene expression analysis

We identified differentially expressed genes using Wilcoxon rank-sum test (function: FindMarkers, min.pct = 0.35, pseudocount.use = 0.01, max.cells.per.ident = 1000, fold-change > 2, adjusted p < 0.01). Marker genes common to all LPC/LLPC neurons were identified by comparison of all LPC/LLPC clusters to all other neurons in the atlas; cell-type-specific markers were identified by comparison of individual LPC/LLPC clusters to other LPC/LLPC neurons. Marker genes were identified for all time points and replicates together. Expression patterns of select markers are shown in Figure S1. Differential analysis of T4/T5 and LLPC neurons in Lop3 and Lop4 for Figure 2 was performed at 48h APF (pseudocount.use = 0.01, fold-change > 3, adjusted p < 0.01).

Generation of null alleles using CRISPR

For side-II and beat-VI, two protospacer sequences targeting the first coding exon were chosen to create a short deletion leading to a frameshift mutation of the protein sequence. For side-IV, two protospacer sequences spanning the whole gene were chosen to create a total 12.9kb deletion. High score protospacer sequence was chosen from UCSC Genome Browser crisprTarget table. Oligos were made from selected gRNA sequences and inserted into pU6-2 vector.⁵³ gRNA plasmid was injected into the vas-Cas9 line (BDSC 51323) via Bestgene Inc. Injected larvae were crossed with balancer lines and F1 progeny was screened for mutation. A frame-shift mutant allele line was established from this single F1 progeny. sgRNA sequences are listed.

side-II[13] (side-II null) deleted sequence(44bp)

TCCGGCGGAGGCAGCAGCATGGGTCCTGGCGGAGGATCCGG

side-IV[4-5] deleted sequence(12.9kb)

AACGCGTATTCGCACCCACACACAAGTGAAGTCGGCTCT.....

GGAACTCTCCGGCACTCCGGTATTCCGGAATTCCGTTGCTCCGGTGCTC

beat-VI[4] (beat-VI null) deleted sequence(19bp): AAGGATACGGAGCCGCCA

MARCM-STaR experiment

MARCM-STaR labels cell morphology and presynaptic machinery (Brp) in single homozygous null mutant neurons in otherwise heterozygous backgrounds.³⁰ The *side-1*[13] allele was recombined with FRT40 for MARCM.⁵⁴ Mitotic recombination was induced at the third instar larva stage with 37°C heat shock for 2–3 min. FLP activated the FRT-flanked stop signal resulting in the expression of R recombinase under GAL4 control. R recombinase then excised sequences encoding the stop codon flanked by R-specific-recombination sites (RSRT). This resulted in the insertion of the V5 tag into Brp and due to the 2A site expression of the linked LexA coding sequence. LexA then induces LexAop-myr-tdTOM to label the cell membranes to visualize cell morphology (Figures S4A and S4B; genotypes in Table S1). Flies were dissected within two days after eclosion. The brains were visualized by immunofluorescence staining as described below.

The T4/T5 GAL4 driver marks all subtypes. In order to classify the identities of T4/T5 MARCM clones, we used the unique dendritic orientation of T4/T5s (i.e. T4c/T5c, dorsal to ventral; T4d/T5d, ventral to dorsal). Brains were mounted to take confocal image stacks along the dorsal to ventral axis, so that the Z-axis in the final volume corresponds to the D-V axis of the compound eye (i.e. the visual field). Images were analyzed in IMARIS to enable 3D visualization. For each T4/T5 dendrite, orientation was determined by the angle of the primary dendritic branch extending away from the axon shaft (i.e. extension away from the axon) and the position of distal tips of the dendrite. T4c/T5c and T4d/T5d dendrites were oriented in opposite directions.

RNAi-MCFO experiment

beat-VI RNAi was driven by LLPC2/3-specific GAL4 driver. To visualize single LLPC2 and LLPC3 neurons we combined MultiColor FlipOut (MCFO) (Nern et al.⁴⁴; Figures 4E and 4H). Heat shock was induced for 8–10 min at 37°C in the mid-pupal stage and the pupae were subsequently reared at 25°C for sparse labeling.

MCFO images for anatomy

Images in Figure 1G show MCFO-labeled cells that were manually segmented and displayed using VVD-viewer. The MCFO images used were acquired by the Janelia FlyLight Project Team using published protocols (protocol (<https://www.janelia.org/project-team/flylight/protocols>)⁴⁴

Cell-type specific labeling of acetylcholine receptor subunits in single neurons

Pupae carrying an LLPC2/3-specific GAL4 driver, beat-VI RNAi, and endogenous conditionally epitope-tagged alleles of nAChR subunits (Sanfilippo, J.Y., and S.L.Z., unpublished data; Figure S4C) were heat shocked at 37°C for 10 min in the mid-pupal stage, and subsequently reared at 25°C for sparse labeling. (see Table S1 for detailed genetics). Brains for analysis were dissected from 1–5 days old files.

Immunohistochemistry for confocal microscopy

Brains were dissected in ice-cold Schneider's Drosophila Medium (GIBCO #21720-024), and fixed in PBS containing 4% paraformaldehyde (PFA) for 25 min at room temperature (RT). Brain tissues were washed three times with PBST (PBS containing 0.5% Triton X-100) and incubated in blocking solution (PBST containing 10% Normal Goat Serum) for at least 2 hours at RT prior to incubation with antibody. Brains were incubated in primary antibody diluted in blocking solution for 2 days at 4°C, washed three times in PBST for 2 hours at RT, then incubated in secondary antibodies diluted in blocking solution for 2 days at 4°C. Brains were washed three times in PBST for 2 hours at RT, then the brains were mounted with Everbrite mounting media (Biotium #23001) or processed for DPX mounting (see below).

Antibody information

Primary antibodies and dilutions used in this study: chicken anti-GFP (1:1000, Abcam #13970), rabbit anti-dsRed (1:200, Clontech #632496), mouse anti-Nc82 (1:40, Developmental Studies Hybridoma Bank (DSHB) Nc82), chicken anti-V5 (1:300, Fortis Life Sciences #A190-118A), rabbit anti-HA (1:200, Cell Signaling Technology #3724), guinea pig anti-Pdm3 (1:20, a gift from John Carlson), mouse anti-Br (1:20, Developmental Studies Hybridoma Bank (DSHB) 25E9.D7), rabbit anti-Ollas (1:10,000; GenScript, Cat# A01658). Secondary antibodies and dilutions used in this study: goat anti-chicken Alexa Fluor 488 (AF488) (1:1000, Invitrogen #A11039), goat anti-rabbit AF568 (Invitrogen #A11011, 1:200), goat anti-guinea pig 568 (1:500, ThermoFisher #A11075), goat anti-mouse AF568 (1:500, ThermoFisher #A11031) goat anti-mouse AF647 (1:500, ThermoFisher #A21235).

Tissue clearing and DPX mounting

Antibody-stained brains were mounted with DPX following Janelia FlyLight protocol (<https://www.janelia.org/project-team/flylight/protocols>). Briefly, after secondary antibody wash as described above, brains were post-fixed with 4% PFA for at least 3 hours in RT. Brains were washed three times in PBS and mounted on polylysine-L coated coverslip. Brains on coverslip were sequentially dehydrated in increasing concentration of ethanol (v/v 50%, 75%, 90%, 100%, 100%, 100%, 10-min each). Dehydrated brains on coverslip were incubated in Xylene (Fisher Scientific, X5-500) three times for 5 minutes for tissue clearing. Then DPX (Electron Microscopy Sciences, #13510) was applied to the coverslip and immediately put on a slide glass. The embedded slide glass was cured in the chemical hood for more than 2 days before imaging. DPX mounting images are noted in the genotype table (Table S1)

Confocal microscopy

Immunofluorescence images were acquired using Zeiss LSM 880 confocal microscope with Zen digital imaging software. Optical sections or maximum intensity projections were level-adjusted, cropped and exported for presentation using ImageJ software (Fiji) or IMARIS 9 (Oxford Instruments). Reported expression patterns were reproducible across three or more biological samples.